

On demand generation of propagation invariant photons with orbital angular momentum

Y. Jerónimo-Moreno, R. Jáuregui¹

¹*Instituto de Física, Universidad Nacional Autónoma de México,
Apartado Postal 20-364, México D. F. 01000, México**

We study the generation of propagation invariant photons with orbital angular momentum by spontaneous parametric down conversion (SPDC) using a Bessel-Gauss pump beam. The angular and conditional angular spectra are calculated for an uniaxial crystal optimized for type I SPDC with standard Gaussian pump beams. It is shown that, as the mean value of the magnitude of the transverse wave vector of the pump beam increases, the emission cone is deformed into two non coaxial cones that touch each other along a line determined by the orientation of the optical axis of the nonlinear crystal. At this location, the conditional spectrum becomes maximal for a pair of photons, one of which is best described by a Gaussian-like photon with a very small transverse wave vector, and the other a Bessel-Gauss photon with a distribution of transverse wave vectors similar in amplitude to that of the incident pump beam. A detailed analysis is then performed of the angular momentum content of SPDC photons by the evaluation of the corresponding transition amplitudes. As a result, we obtain conditions for the generation of heralded single photons which are approximately propagation invariant and have orbital angular momentum. A discussion is given about the difficulties in the interpretation of the results in terms of conservation of optical orbital angular momentum along the vector normal to the crystal surface. The angular spectra and the conditional angular spectra are successfully compared with available experimental data recently reported in the literature.

PACS numbers: 42.50.-p, 42.65.Lm

* rocio@fisica.unam.mx

I. INTRODUCTION

In the last two decades there has been huge advances in the generation of structured light beams with several spatial and dynamical features. Probably the best known examples correspond to beams with orbital angular momentum (OAM), e. g. Laguerre [1] and Bessel beams [2], though other possibilities with diverse transverse [3, 4] and longitudinal structure [5] are not less interesting. The richness of structured beams is inherited to several optical phenomena. Here we shall focus on spontaneous parametric down conversion (SPDC).

SPDC from structured beams can be useful for the implementation of quantum information protocols for which the encoding variables may be different from polarization, linear momentum or frequency of the photons. In quantum optics, two-photon states entangled in polarization, usually generated via a SPDC process, have become the most widely used entangled systems. In this case, the two photons in a pair usually have one of two orthogonal polarization directions [6]. In most cases, the description of the system is made in a Hilbert space of just two-dimensions, though the role of the other degrees of freedom of the photon should not be ignored in general. Quantum-enhanced technologies demand systems consisting of multiple entangled states, as well as quantum states entangled in multiple dimensions. The latter may, for instance, improve the communication channel efficiency in quantum cryptography [7]. The generation of two-photon states with multi-dimensional entanglement has been shown to be feasible, and the challenge to control it is the main subject of many theoretical and experimental current studies.

One way to produce entanglement in a Hilbert space with dimension greater than two, is by taking advantage of the diversity of spatial modes of the electromagnetic (EM) field. Furthermore, from modes with well defined OAM, it is possible to generate two-photon states entangled in this degree of freedom, which have a discrete dimensionality as a result of the quantization of angular momentum. The first experimental demonstration of OAM entanglement in photon pairs generated by SPDC was reported in 2001 [8] and since then several similar sources have been implemented.

The role of the linear and nonlinear electromagnetic response of the material used for SPDC on the pump beam is essential for a precise description of the expected quantum correlations of the photon pairs. There is not a unique basis set to perform such a description. Most studies of SPDC rely on the use of the plane EM wave expansion. Accordingly, polarization, linear momentum and frequency become the natural degrees of freedom, and the effects of birefringence on these variables through the type I and type II phase matching conditions restricts the possibility of SPDC by conventional nonlinear crystals. For pump beams with OAM, one may describe the system as a continuum superposition of plane EM waves, or perform the description in terms of modes with OAM. In the latter case it must be recognized that the birefringence of SPDC crystals is able to modify both the polarization and the OAM of the modes that propagate in them [9]. As a consequence, OAM conservation in SPDC does not necessarily hold [10]. Most studies of this kind of effects take as starting point an effective scalar treatment of the EM field and the paraxial description of the pump mode, though going beyond these approximations may lead to observable effects [10–12].

As already reported in Ref. [13], for wide crystals, the plane-wave spectrum from the pump beam results in a multiplicative factor for the transition amplitude of the generated two-photon state. This opens the possibility of using SPDC to generate photons with general properties inherited from the pump photons. In the case of a propagation invariant Bessel pump beam, this could lead to the generation of propagation invariant photons with OAM. In the present work, we theoretically study the circumstances under which this process is feasible and compare our analysis with available experimental results [14]. Notice that in the implementation of many quantum protocols, the photons with selected properties are generated in a given space region and are processed in a different location. Propagation invariant photons have an angular spectra restricted to a cone in wave vector space. Its perpendicular radius can be optimized for an efficient coupling to optical fibers [15]. Besides, they possess the self healing property [16], that is they tend to reform during propagation in spite of blocking part of them. This property makes them robust in scattering and turbulent environments.

The article is organized as follows. In section II, we describe general features of type I SPDC involving structured vectorial beams in a birefringent medium. In section III, this formalism is applied to the case of a Bessel-Gauss pump beam. Explicit analytical expressions and numerical results for the angular spectrum are given and compared with experimental results. The angular momentum properties of the photon pair are also analyzed, including a discussion on the pertinence of studying its conservation in the SPDC process. Finally, we outline conclusions derived from this study.

II. SPDC OF STRUCTURED EM FIELDS.

Spontaneous parametric down conversion focus on the evolution of an initial state of the quantum electromagnetic field that corresponds to a coherent state for a given pumping mode κ_p with no other occupied mode $|0; \alpha_{\kappa_p}\rangle$, under

the $\hat{\mathcal{H}}_{SPDC}$ Hamiltonian [17],

$$\hat{\mathcal{H}}_{SPDC}|0; \alpha_{\kappa_p}\rangle = \frac{1}{2} \sum_{r,l,t} \int d^3r \chi_{r,l,t}^{(2)} \hat{\mathbf{E}}_r^{(+)} \hat{\mathbf{E}}_l^{(+)} \hat{\mathbf{E}}_t^{(-)} |0; \alpha_{\kappa_p}\rangle. \quad (1)$$

Here $\chi_{r,l,t}^{(2)}$ denotes the second order electric susceptibility of the nonlinear media. The operators $\hat{\mathbf{E}}_l^{(\pm)}$ are usually written as a series expansion on a basis formed by EM monochromatic modes that satisfy the adequate boundary conditions. $\hat{\mathbf{E}}_l^{(+)}$ ($\hat{\mathbf{E}}_l^{(-)}$) is the electric field operator that includes the modes with frequency ω that propagate with a time dependence $e^{-i\omega t}$ ($e^{i\omega t}$). The best known example of $\hat{\mathbf{E}}$ corresponds to the EM field confined within a rectangular cavity of volume V in otherwise free space:

$$\begin{aligned} \hat{\mathbf{E}} &= \hat{\mathbf{E}}^{(+)} + \hat{\mathbf{E}}^{(-)} \\ &= \sum_s \int d\omega d^3\mathbf{k} \mathcal{N}_{\mathbf{k}} \delta(\sqrt{k_x^2 + k_y^2 + k_z^2} - \omega/c) \left[e^{i(\mathbf{k}\cdot\mathbf{r} - \omega t)} \hat{e}_{\mathbf{k},s} \hat{a}_{\mathbf{k},s}^\dagger + e^{-i(\mathbf{k}\cdot\mathbf{r} - \omega t)} \hat{e}_{\mathbf{k},s}^* \hat{a}_{\mathbf{k},s} \right], \end{aligned} \quad (2)$$

$\hat{e}_{\mathbf{k},s}$ denotes the unitary vectors giving the mode polarization s , c is the velocity of light in vacuum and $\mathcal{N}_{\mathbf{k}}$ is the normalization factor, $\mathcal{N}_{\mathbf{k}} = \sqrt{2\pi\hbar/\omega_{\mathbf{k}}V}$. For other boundary conditions or in the presence of a media that modifies the dispersion relations, each electromagnetic mode κ can still be expressed in terms of its properly normalized plane-wave spectrum $\mathfrak{E}_{\kappa,l}^{(+)}(s, \mathbf{k}_x, \mathbf{k}_y; \omega)$. In this case,

$$\begin{aligned} \hat{\mathcal{H}}_{SPDC}|0; \alpha_{\kappa_p}\rangle &= \sum_{\kappa^s, \kappa^i} \left[\frac{1}{2} \sum_{r,l,t} \int d^6k_{\perp} \chi_{r,l,t}^{(2)} \mathfrak{E}_{\kappa^s,r}^{(+)}(s^s, \mathbf{k}_x^s, \mathbf{k}_y^s; \omega^s) \mathfrak{E}_{\kappa^i,l}^{(+)}(s^i, \mathbf{k}_x^i, \mathbf{k}_y^i; \omega^i) \mathfrak{E}_{\kappa^p,t}^{(-)}(s^p, \mathbf{k}_x^p, \mathbf{k}_y^p; \omega^p) \right. \\ &\quad \left. \times \int d^3r e^{i(\Delta\mathbf{k}\cdot\mathbf{r} - \Delta\omega t)} \hat{a}^\dagger(s^s, \mathbf{k}_x^s, \mathbf{k}_y^s; \omega^s) \hat{a}^\dagger(s^i, \mathbf{k}_x^i, \mathbf{k}_y^i; \omega^i) \alpha_{\kappa^p} |0; \alpha_{\kappa^p}\rangle \right]. \end{aligned} \quad (3)$$

Here d^6k_{\perp} encloses the transverse momentum differentials for each field; $\Delta\mathbf{k}$ denotes the vectorial mismatch term $\Delta\mathbf{k} = \mathbf{k}^p - \mathbf{k}^s - \mathbf{k}^i$, and $\Delta\omega = \omega^p - \omega^s - \omega^i$. Each $\{\kappa^s, \kappa^i\}$ term in this expansion determines the probability amplitude for the creation of a photon in the signal (idler) mode κ^s (κ^i) together with the annihilation of a photon in the coherent pumping state. The time integral of this equation gives an approximate expression, valid within first order perturbation theory, of the time evolved SPDC state

$$\begin{aligned} |\Psi(t)\rangle &= |0; \alpha_{\kappa_p}\rangle + \sum_{\kappa^s, \kappa^i} \left[\frac{1}{2} \sum_{r,l,t} \int d^6k_{\perp} \chi_{r,l,t}^{(2)} \mathfrak{E}_{\kappa^s,r}^{(+)}(s^s, \mathbf{k}_x^s, \mathbf{k}_y^s; \omega^s) \mathfrak{E}_{\kappa^i,l}^{(+)}(s^i, \mathbf{k}_x^i, \mathbf{k}_y^i; \omega^i) \mathfrak{E}_{\kappa^p,t}^{(-)}(s^p, \mathbf{k}_x^p, \mathbf{k}_y^p; \omega^p) \right. \\ &\quad \left. \times \int d^3r e^{i(\Delta\mathbf{k}\cdot\mathbf{r} - \Delta\omega t/2)} \text{sinc}(\Delta\omega t/2) \hat{a}^\dagger(s^s, \mathbf{k}_x^s, \mathbf{k}_y^s; \omega^s) \hat{a}^\dagger(s^i, \mathbf{k}_x^i, \mathbf{k}_y^i; \omega^i) \alpha_{\kappa^p} |0; \alpha_{\kappa^p}\rangle \right]. \end{aligned} \quad (4)$$

In this work we shall present an analysis for a type-I SPDC, with this configuration, for a quasi monochromatic pump beam that propagates in an uniaxial crystal with symmetry axis \mathbf{a} and permeability coefficients ϵ_{\parallel} and ϵ_{\perp} parallel and transversal to the optical axis respectively. The electric field associated to the extraordinary waves is:

$$\mathfrak{E}_{e,\kappa}(\mathbf{k}_x, \mathbf{k}_y; \omega) = \left[-\frac{c^2}{\epsilon_{\perp}\omega^2} \mathbf{k}^e (\mathbf{a} \cdot \mathbf{k}^e) + \mathbf{a} \right] \mathcal{N}_e \alpha(\omega) \tilde{\psi}_{\kappa}(\mathbf{k}_x, \mathbf{k}_y), \quad (5)$$

with $\tilde{\psi}_{\kappa}(\mathbf{k}_x, \mathbf{k}_y)$ the 2-dimensional Fourier transform of the pump beam evaluated at the crystal surface and $\alpha(\omega)$ its spectral envelop. As for the generated photons,

$$\mathfrak{E}_{o,\mathbf{k}_x^0, \mathbf{k}_y^0}(\mathbf{k}_x, \mathbf{k}_y; \omega^0) = \mathbf{a} \times \mathbf{k}^0 \mathcal{N}_o \delta(\mathbf{k}_x - \mathbf{k}_x^0) \delta(\mathbf{k}_y - \mathbf{k}_y^0), \quad (6)$$

if they are described by ordinary vectorial plane waves with wave vector \mathbf{k}^0 and frequency ω^0 . In Eqs. (5-6) \mathcal{N}_e and \mathcal{N}_o are the normalization factors, and the vectors \mathbf{k}^e and \mathbf{k}^o satisfy the extraordinary and the ordinary dispersion relations, respectively. Notice that, as expected the electric field of the ordinary modes is perpendicular to both the optical axis \mathbf{a} and the wave vector \mathbf{k} , while the electric field of the extraordinary modes has a component along the optical axis \mathbf{a} and a component along the wave vector \mathbf{k} in a combination that guarantees the fulfillment of the Maxwell equations in the birefringent media.

For a wide crystal the state of the electromagnetic field at asymptotic times can be written as

$$|\Psi\rangle = |0; \alpha_{\kappa_p}\rangle + \frac{\pi}{i\hbar} \int d\omega^s \int d\omega^i \int d^2k_{\perp}^s d^2k_{\perp}^i \mathcal{N}_p \mathcal{N}_s \mathcal{N}_i \alpha(\omega^s + \omega^i) \mathcal{X} F(\mathbf{k}_x^s, \mathbf{k}_y^s; \omega^s, \mathbf{k}_x^i, \mathbf{k}_y^i; \omega^i) |0; \alpha_{\kappa_p}; 1_s; 1_i\rangle. \quad (7)$$

The factor \mathcal{X} results from the contraction of the nonlinear susceptibility tensor $\chi_{r,l,q}^{(2)}$ with the polarization vectors, while the wave vector joint amplitude is defined as

$$F(\mathbf{k}_x^s, \mathbf{k}_y^s; \omega^s, \mathbf{k}_x^i, \mathbf{k}_y^i; \omega^i) = \tilde{\psi}_\kappa(\mathbf{k}_x^i + \mathbf{k}_x^s, \mathbf{k}_y^i + \mathbf{k}_y^s) \text{sinc}(L\Delta\mathbf{k}_z/2) \exp(i\Delta\mathbf{k}_z L/2). \quad (8)$$

In this equation L denotes the crystal length and $\Delta\mathbf{k}_z = \mathbf{k}_z^p - \mathbf{k}_z^s - \mathbf{k}_z^i$, with each \mathbf{k}_z evaluated in terms of the vectors \mathbf{k}_\perp using the adequate dispersion relation.

The product

$$\mathfrak{F}(\mathbf{k}_x^s, \mathbf{k}_y^s; \omega^s, \mathbf{k}_x^i, \mathbf{k}_y^i; \omega^i) = \alpha(\omega^s + \omega^i) g F(\mathbf{k}_x^s, \mathbf{k}_y^s; \omega^s, \mathbf{k}_x^i, \mathbf{k}_y^i; \omega^i), \quad g = \mathcal{N}_p \mathcal{N}_s \mathcal{N}_i \mathcal{X}, \quad (9)$$

yields the probability amplitude to generate the idler and signal photons. It determines $|\Psi\rangle$ to first order in the perturbation theory. In general, $\mathfrak{F}(\mathbf{k}_x^s, \mathbf{k}_y^s; \omega^s, \mathbf{k}_x^i, \mathbf{k}_y^i; \omega^i)$ will be non negligible for continuous sets of the wave vectors \mathbf{k}_\perp , so that the wave function cannot be factorized, and entanglement in continuous and discrete polarization variables can be expected.

Equation (8) shows how the transverse momentum conservation condition $\mathbf{k}_\perp^p = \mathbf{k}_\perp^i + \mathbf{k}_\perp^s$ induces the transfer of the plane-wave spectrum from the pump beam to the two-photon state [13]. If, for instance, one of the photons in the pair is projected in a state with a well defined value of \mathbf{k}_\perp , the other photon will have a plane-wave spectrum proportional to the pump spectrum with an argument modified by a constant additive term. Note, however, that \mathfrak{F} is also modulated both by the longitudinal phase matching factor (which depends on \mathbf{k}_\perp^i and \mathbf{k}_\perp^s by the dispersion relations) and by the nonlinear response term \mathcal{X} . Thus, the conditions under which the idler and/or signal photons inherit general features of the pump beam plane-wave spectrum are not evident.

An important function to calculate is the angular spectrum (AS), which describes the distribution of signal photons in the wave vector domain, and is defined as

$$R_s(\mathbf{k}_0^s) = \int d\omega^i \int d^2k_\perp^i |\mathfrak{F}(\mathbf{k}_{x,0}^s, \mathbf{k}_{y,0}^s; \omega^s, \mathbf{k}_x^i, \mathbf{k}_y^i; \omega^i)|^2. \quad (10)$$

The conditional angular spectrum (CAS), which is a function of \mathbf{k}_\perp^s and $\mathbf{k}_{\perp,0}^i$, is defined as:

$$R_c(\mathbf{k}_\perp^s, \mathbf{k}_{\perp,0}^i; \omega_0^i) = \int d\omega^s |\mathfrak{F}(\mathbf{k}_x^s, \mathbf{k}_y^s; \omega^s, \mathbf{k}_{x,0}^i, \mathbf{k}_{y,0}^i; \omega_0^i)|^2, \quad (11)$$

and represents the probability to detect an idler photon with wave vector $\mathbf{k}_{\perp,0}^i$ and frequency ω_0^i in coincidence with a signal photon with wave vector \mathbf{k}_\perp^s . Under a realistic situation involving small but finite transverse dimensions of the pump beam and an usually wide but not so long crystal, there is a set of relevant pump wave vectors \mathbf{k}^p that are close to satisfy the phase matching condition $\Delta\mathbf{k}_z = 0$ for a given idler wave vector \mathbf{k}^i .

III. SPDC FOR A PROPAGATION INVARIANT PUMP WITH CIRCULAR CYLINDER SYMMETRY.

The solutions of the scalar wave equation in free space that preserve its amplitude along a main propagation axis are said to be propagation invariant. If the main propagation axis of the beam is chosen to be the z -axis, their scalar plane-wave spectrum $\tilde{\psi}_\kappa(\mathbf{k}_x, \mathbf{k}_y)$ is confined into a cone, that is, the transverse wave number κ_\perp^p of these beams, under ideal conditions, takes a unique value,

$$\tilde{\psi}_\kappa(\mathbf{k}_x, \mathbf{k}_y) = \Phi_\kappa(\varphi_{\mathbf{k}_\perp}) \delta(\mathbf{k}_\perp - \kappa_\perp) / \kappa_\perp. \quad (12)$$

Approximate realizations of propagation invariant beams in the laboratory correspond to superpositions of waves with vectors \mathbf{k} in a narrow conic shape volume:

$$\delta(\mathbf{k}_\perp - \kappa_\perp) \rightarrow \frac{1}{W\sqrt{2\pi}} \text{Exp} [-(\mathbf{k}_\perp - \kappa_\perp)^2 / 2W^2], \quad W \ll \kappa_\perp. \quad (13)$$

with W a waist parameter around the non-zero mean κ_\perp value.

Propagation invariant beams with well defined orbital angular momentum are known as Bessel modes. The corresponding angular spectra spectra is given by

$$\Phi_\ell(\varphi_{\mathbf{k}_\perp}) = i^\ell e^{i\ell\varphi_{\mathbf{k}_\perp}}, \quad (14)$$

so that the modulus of $\tilde{\psi}_\kappa(\mathbf{k}_x, \mathbf{k}_y)$ is not dependent on $\varphi_{\mathbf{k}_\perp}$. Their realizations in terms of narrow cones in wave vector space are called Bessel-Gauss modes.

Consider a linearly polarized Bessel-Gauss mode generated in free space. The beam is sent with its main direction of propagation along the z -axis, *i. e.*, perpendicular to a birefringent crystal surface, and with a polarization vector within the extraordinary plane. In the case the optical axis is taken as $\mathbf{a} = (0, a_y, a_z)$, the angular spectra of the scalar pump beam \mathfrak{E}^{sc} can be approximately expressed as [18]:

$$\mathfrak{E}_{\mathbf{k}_\perp, \ell, \omega}^{sc} \sim \mathcal{E}^{sc} \frac{e^{-(\mathbf{k}_\perp - \kappa_\perp^p)^2/2W^2}}{\kappa_\perp^p} e^{i\ell\varphi_{\mathbf{k}_\perp^p}} \hat{\mathbf{e}}_y. \quad (15)$$

Inside the crystal the extraordinary mode that will give rise to the SPDC process evolves according to Eq. (5) with an amplitude determined approximately by $\mathfrak{E}^{sc} \cdot \mathfrak{E}_\kappa$. Notice that, in general the vectorial factors $[-(c^2/\epsilon_\perp \omega^2) \mathbf{k}^e (\mathbf{a} \cdot \mathbf{k}^e) + \mathbf{a}]$ introduce anisotropy along the z axis.

For uniaxial media, the nonlinear optical susceptibilities $\chi_{r,l,q}^{(2)}$ are usually reported in the reference frame where the birefringent axis is taken as the z -axis. In this frame we can evaluate \mathcal{X} , and then translate the results in terms of the rotated wave vector \mathbf{k} . Let us take as a particular example the case of a beta barium borate (BBO) crystal and a type I phase-matching configuration. The symmetry of the crystal is such that, in the crystal natural frame ($\hat{\mathbf{e}}_3 = \mathbf{a}$):

$$\mathcal{X} \approx -d_{22} [\tilde{\mathbf{e}}_x^0 \tilde{\mathbf{e}}_y^0 + \tilde{\mathbf{e}}_y^0 \tilde{\mathbf{e}}_x^0] \tilde{\mathbf{e}}_x^e + [\tilde{\mathbf{e}}_x^0 \tilde{\mathbf{e}}_x^0 - \tilde{\mathbf{e}}_y^0 \tilde{\mathbf{e}}_y^0] \tilde{\mathbf{e}}_y^e. \quad (16)$$

with $d_{22} \sim 2.2 \text{ pm/V}$ the element of the contracted nonlinear matrix d_{ij} [19]. In the case of vectorial electromagnetic beams in birefringent crystals, the components of the electric field depend on the components of the wave vector, Eqs. (5-6), so that,

$$\mathcal{X} \approx -d_{22} \frac{\omega^s}{c} \frac{\omega^i}{c} \tilde{k}_z^p \left[[-\tilde{k}_y^s \tilde{k}_x^i - \tilde{k}_x^s \tilde{k}_y^i] \tilde{k}_x^p + [\tilde{k}_y^s \tilde{k}_y^i - \tilde{k}_x^s \tilde{k}_x^i] \tilde{k}_y^p \right], \quad (17)$$

with $\tilde{\mathbf{k}}$ the rotated wave vector in the crystal reference frame.

For the system under consideration, if the crystal is wide and the pump beam satisfies the paraxial condition, $k_\perp^p \ll \omega/c$, the conservation of transversal momentum makes reasonable that both the relevant ordinary and extraordinary modes are quasi parallel to the incident beam. All these considerations make feasible to replace the vectorial factor \mathcal{X} by its effective value \mathcal{X}_{eff} . This implies that under these conditions, the SPDC process of structured paraxial beams will be determined just by the scalar potential $\tilde{\psi}^p$ modulated by the longitudinal phase matching factor. Notice, however, that these considerations also suggest that the usage of vectorial non paraxial beams could open new perspectives in SPDC.

A. SPDC angular spectrum and conditional angular spectrum for paraxial scalar Bessel beams.

In this subsection we calculate the AS, Eq. (10), and the CAS, Eq. (11), functions for a quasi paraxial scalar Bessel pump beam, Eq. (15), under the conditions described in the last paragraph.

The first observation is that the modulus of the joint amplitude $|\mathfrak{F}|$, Eq. (9), in the scheme where Eq. (15) is valid, does not depend on ℓ . So that the AS and CAS are ℓ independent [20].

We assume type-I SPDC in an uniaxial birefringent crystal with its optical axis given by $\mathbf{a} = (0, a_y, a_z)$. For degenerated emission, *i.e.*, $\omega^p = \omega = 2\omega^s = 2\omega^i$, the emitted photons dispersion relation is

$$k_{z,b}^O = \sqrt{\epsilon_\perp \omega^2/4c^2 - (\mathbf{k}_\perp^b)^2} \quad b = i, s, \quad (18)$$

with the ordinary refraction index $n_o = \sqrt{\epsilon_\perp}$. The dispersion relation for the pump wave which evolves in the extraordinary plane is

$$k_z^E(\mathbf{k}_\perp, \omega) = -\beta \mathbf{a} \cdot \mathbf{k}_\perp + \frac{\omega}{c} n_{eff} \sqrt{1 - \frac{k_\perp^2 c^2}{\omega^2}} \eta, \quad (19)$$

$$n_{eff} = \sqrt{\frac{\epsilon_\perp \epsilon_\parallel}{\epsilon_\perp + \Delta \epsilon a_z^2}}, \quad \beta = \frac{\Delta \epsilon a_z}{\epsilon_\perp + \Delta \epsilon a_z^2}, \quad \eta = \frac{1}{\epsilon_\perp + \Delta \epsilon a_z^2}, \quad (20)$$

where $\Delta \epsilon = \epsilon_\parallel - \epsilon_\perp$. In the limit of normal incidence, this equation reduces to the expression of the effective refractive index experienced by a paraxial pumping extraordinary wave, $k_z^E(\mathbf{k}_\perp \sim \mathbf{0}) = n_{eff} \omega/c$. For quasi normal incidence, the deviation angle ρ_{wo} of the Poynting vector with respect to the wavefront inside the crystal can be approximated by $\tan \rho_{wo} \sim \beta a_y$. So that β measures the so called walk-off effect on the pump beam [21–24]. The η term in Eq. (19) gives rise to astigmatic effects [11].

1. SPDC angular spectrum.

In order to obtain approximate expressions for the AS function, we make a first order Taylor description of the phase mismatch term,

$$\Delta k_z \sim \tilde{\kappa} - \mathbf{d} \cdot (\mathbf{k}_\perp^s + \mathbf{k}_\perp^i), \quad (21)$$

with

$$\tilde{\kappa} = (\omega/c)(n_{eff} - n_o) + (2c/n_o\omega)(\mathbf{k}_\perp^s)^2, \quad \mathbf{d} = \beta \mathbf{a}_\perp + (2c/n_o\omega)\mathbf{k}_\perp^s. \quad (22)$$

Writing the pump integration variable \mathbf{k}_\perp^p in polar coordinates, and performing a rotation of the integration variable by an angle $\theta_r = \arccos(d_x/|\mathbf{d}|)$, the expression for the AS can be written in terms of a single integral:

$$R_s(k_x^s, k_y^s) \sim |g\alpha(\omega_p)|^2 e^{-\sigma_{AS}^{-2}((\mathbf{k}_\perp^s)^2 - r_{AS}^2)} \int_0^{2\pi} \text{Exp} \left[-\frac{(\gamma L)^2}{2} (|\mathbf{d}| \kappa_\perp^p \sin \varphi_p - \tilde{\kappa})^2 \right] d\varphi_p, \quad (23)$$

$$r_{AS}^2 = \frac{1}{2} \left(\frac{n_o\omega}{c} \right)^2 \left(1 - \frac{n_{eff}}{n_o} \right), \quad \sigma_{AS}^{-2} = 2(\gamma L c / n_o \omega)^2.$$

Note that r_{AS} depends in general on the wavelength. To obtain this expression, we have approximated the function $\text{sinc}(x)$ by a Gaussian function $\exp[-(\gamma x)^2]$, $\gamma = 0.4393$. We have also taken the limit $W \rightarrow 0$ with the restriction of a finite pump intensity.

According to Eq. (23), for $\kappa_\perp^p \ll (\omega/c)|n_{eff} - n_o|$, the AS is concentrated in a cone given by the condition $k_\perp^s = (n_o\omega/\sqrt{2}c)\sqrt{1 - n_{eff}/n_o} = r_{AS}$ for a negative birefringent crystal (a similar expression is obtained for Gaussian pump beams [25]). The cone width is approximately given by $\sigma_{AS}^{1/2}$.

Since

$$\tilde{\kappa} = \left(\frac{2c}{n_o\omega} \right) ((k_\perp^s)^2 - r_{AS}^2) \quad (24)$$

for $\kappa_\perp^p \ll (\omega/c)|n_{eff} - n_o|$, $\tilde{\kappa} \sim 0$. That is, as expected, for small values of κ_\perp^p the angular spectrum will be similar to that obtained from Gaussian pump beams [25].

As κ_\perp^p increases, the restriction $k_\perp^s \sim r_{AS}$ is relaxed since the contribution of the phase matching integral over the angle of wave vectors components of the pump beam in Eq. (23)

$$\int_0^{2\pi} \text{Exp} \left[-\frac{(\gamma L)^2}{2} (|\mathbf{d}| \kappa_\perp^p \sin \varphi_p - \tilde{\kappa})^2 \right] d\varphi_p, \quad (25)$$

is more relevant. This integral makes explicit that the phase matching condition involves the superposition effects of the wave vectors that arrive on the crystal in an isotropic way with respect to the crystal surface, but are not isotropically distributed with respect to the optical axis. In fact, this integral gives rise to anisotropic effects in the AS due to the dependence of

$$|\mathbf{d}| = \left(\frac{2c}{n_o\omega} \right) \left[k_x^{s2} + \left(k_y^s + \frac{n_o\omega\beta a_y}{2c} \right)^2 \right]^{1/2} \quad (26)$$

on the orientation of the axis $\mathbf{a} = (0, a_y, a_z)$. This dependence suggests that the effects of this integral on the AS will yield structures that are not centered at the origin, but displaced in the direction of the Y -axis. This displacement would be absent if κ_\perp^p were zero, *e. g.*, for a Gaussian pump beam. Notice that κ_\perp^p appears in the integrand in a combination $\kappa_\perp^p \sin \varphi_p$. So that, depending on the sign of the sine function in the exponent, the values of $\tilde{\kappa}$ over which the integral is relevant will be either positive (yielding greater values of k_\perp^s with respect to r_{AS}) or negative (yielding lower values of k_\perp^s with respect to r_{AS}). From these considerations we expect that the structure of the AS will now involve two non homogenous and non concentric cones with different radii. The actual displacement of the center of these cones can be estimated by evaluating the zeros of the exponent in the integral given in Eq. (25) for the particular case $k_x^s = 0$. We obtain that, for a negative birefringent crystal and for $|n_o\omega\beta a_y/2c| \sim r_{AS} \gg \kappa_\perp^p$, the cone with quasi circular transverse structure and the biggest radius R_+ has an axis that passes through the point $(0, A_+)$ with

$$\begin{aligned} R_+ &\sim r_{AS} - \frac{\kappa_\perp}{2} \left(1 + \frac{n_o\omega\beta a_y}{2cr_{AS}} - \frac{\kappa_\perp}{2r_{AS}} \right), \\ A_+ &\sim -\frac{\kappa_\perp}{2} \left(1 + \frac{n_o\omega\beta a_y}{2cr_{AS}} - \frac{\kappa_\perp}{2r_{AS}} \right), \end{aligned} \quad (27)$$

while the axis of the cone with lowest transverse radius R_- passes through $(0, A_-)$ with

$$\begin{aligned} R_- &\sim r_{AS} - \frac{\kappa_\perp}{2} \left(1 - \frac{n_o \omega \beta a_y}{2cr_{AS}} + \frac{\kappa_\perp}{2r_{AS}} \right), \\ A_- &\sim + \frac{\kappa_\perp}{2} \left(1 + \frac{n_o \omega \beta a_y}{2cr_{AS}} - \frac{\kappa_\perp}{2r_{AS}} \right). \end{aligned} \quad (28)$$

The two emission cones almost touch each other along the direction defined by the wave vector $\sim (0, -r_{AS} + \kappa/2, k_z)$ for an optical axis $\mathbf{a} = (0, a_y, a_z)$. If the optical axis were located at the X - Z plane the direction at which the cones would touch each other would be defined by a wave vector contained in the K_x - K_z plane. The double conical structure of the AS reflects both the anisotropy of the wave vectors in the incoming Bessel pump beam with respect to the optical axis and walk-off effects encoded in βa_y term of the extraordinary beam dispersion relation.

Our theoretical scheme has been implemented using parameters from the reported experimental setup in Ref. [14]. We consider a SPDC source based on a BBO crystal, cut for type-I phase matching for degenerated emission and normal incidence of a pump quasi plane wave with wavelength centered at 406.8 nm ($\theta_a = 29.3^\circ$, optical axis $\mathbf{a} = (0, \sin \theta_a, \cos \theta_a)$). The numerical simulations consider monochromatic Bessel-Gauss pump beams with a waist $W = 0.0007 \mu\text{m}^{-1}$ and three different values for the transverse wave number parameter $\kappa_\perp^p = 0.05, 0.09, 0.15 \mu\text{m}^{-1}$. They are performed both using the complete expression of the transition rate Eq.(10) without resorting approximations to the dispersion relations, Figs. 1a-1c, and using the analytic expression, Eq. (23), Figs. 1b-1d, for two different crystal lengths. The AS function for $\kappa_\perp^p = 0.05 \mu\text{m}^{-1}$ shows an asymmetry compatible with the experimental results reported in Ref.[14]. In this case, the AS function is concentrated in a cone of radius $0.49 \mu\text{m}^{-1}$ and width between $\sim 0.01 - 0.03 \mu\text{m}^{-1}$ dependent on k_y^s/k_x^s . Both radius and width are within the expectations described above. As κ_\perp^p increases, the anisotropy is more visible and the spectrum is better described by two non concentric cones that almost touch each other along a line determined by the orientation of the optical axis of the nonlinear crystal. This is illustrated in Fig.(1a)B where $\kappa_\perp^p = 0.09 \mu\text{m}^{-1}$ and Fig.(1a)C with $\kappa_\perp^p = 0.15 \mu\text{m}^{-1}$. As the crystal length is increased the regions where the AS has significant values are smaller and the anisotropy associated to the extraordinary pump beam dispersion relation is more evident. This, along with the oscillatory behavior of the sinc function, leads to a higher structured landscape for the AS function, which, nevertheless is still concentrated in two narrow non concentric cones. The radius of the external cone increases as κ_\perp increases while the radius of the internal cone decreases as κ_\perp decreases; all this is in accordance to the expectations described above. By comparing Figs. 1a with Figs. 1b and Figs. 1c with Figs. 1d we can conclude that the analytic expression, Eq. (23), reproduces the general features of the AS function for κ_\perp^p at least as high as $0.15 \mu\text{m}^{-1}$. The displacement of the centers of the AS cones and their radii are also correctly estimated by Eqs. (27-28).

2. SPDC conditional angular spectrum.

Now we shall study the probability to detect an idler photon with wave vector $\mathbf{k}_{\perp,0}^i$ in coincidence with a signal photon with wave vector \mathbf{k}_\perp^s in terms of the conditional angular spectrum, Eq. (11). Using the same approximations for the phase matching function and phase mismatch term, it is possible to obtain an useful expression for the CAS function. In this case we do not take the limit $W \rightarrow 0$ to make more explicit the role of this parameter in the expected CAS to be measured in the laboratory. Replacing Eq. (8), Eq. (15) and Eq. (21) in Eq. (11), for degenerate SPDC, we obtain:

$$R_c(\mathbf{k}_\perp^s, \omega^s; \mathbf{k}_\perp^i, \omega^i) \sim \frac{|g\alpha(\omega^p)|^2}{2\pi W^2} e^{-(|\mathbf{k}_\perp^s - \mathbf{K}_\perp^0|^2 - \mathcal{R}_\mathbf{k}^2)/2W_{eff}^2}, \quad (29)$$

with

$$\begin{aligned} W_{eff}^{-2} &= W^{-2} + \gamma^2 L^2 \beta^2 (\mathbf{a} \cdot \hat{\mathbf{k}}_\perp)^2, \\ \mathbf{K}_\perp^0 &= -\frac{W_{eff}^2}{W^2} \mathbf{k}_\perp^i + (\gamma L W_{eff})^2 \left(\frac{\omega}{c} (n_{eff} - n_o) - \beta \mathbf{a} \cdot \mathbf{k}_\perp^i \right) \left(\frac{2c}{n_o \omega} \mathbf{k}_\perp^i - \beta \mathbf{a} \right), \\ \mathcal{R}_\mathbf{k}^2 &= \frac{W_{eff}^2}{W^2} (\kappa_\perp^p)^2 + (\mathbf{k}_\perp^i)^2 \left[\frac{W_{eff}^4}{W^4} - \frac{W_{eff}^2}{W^2} \right] + 2(\gamma L W_{eff})^2 \left(\frac{\omega}{c} (n_{eff} - n_o) - \beta \mathbf{a} \cdot \mathbf{k}_\perp^i \right) \left(\frac{2c}{n_o \omega} (\mathbf{k}_\perp^i)^2 - \beta \mathbf{a} \cdot \mathbf{k}_\perp^i \right) \\ &\quad - \left(\frac{2c}{n_o \omega} (\mathbf{k}_\perp^i)^2 - \beta \mathbf{a} \cdot \mathbf{k}_\perp^i \right)^2 (\gamma L W_{eff})^2 \left[1 - (\gamma L W_{eff})^2 \left| \frac{2c}{n_o \omega} \mathbf{k}_\perp^i - \beta \mathbf{a} \right|^2 \right]. \end{aligned} \quad (30)$$

If the crystal is not too long $W_{eff} \sim W$, $\mathbf{K}_\perp^0 = -\mathbf{k}_\perp^i$ and $\mathcal{R}_\mathbf{k} \sim k_\perp^0$; as the length of the crystal increases the longitudinal phase matching condition becomes more relevant and two types of corrections arises. One of them is

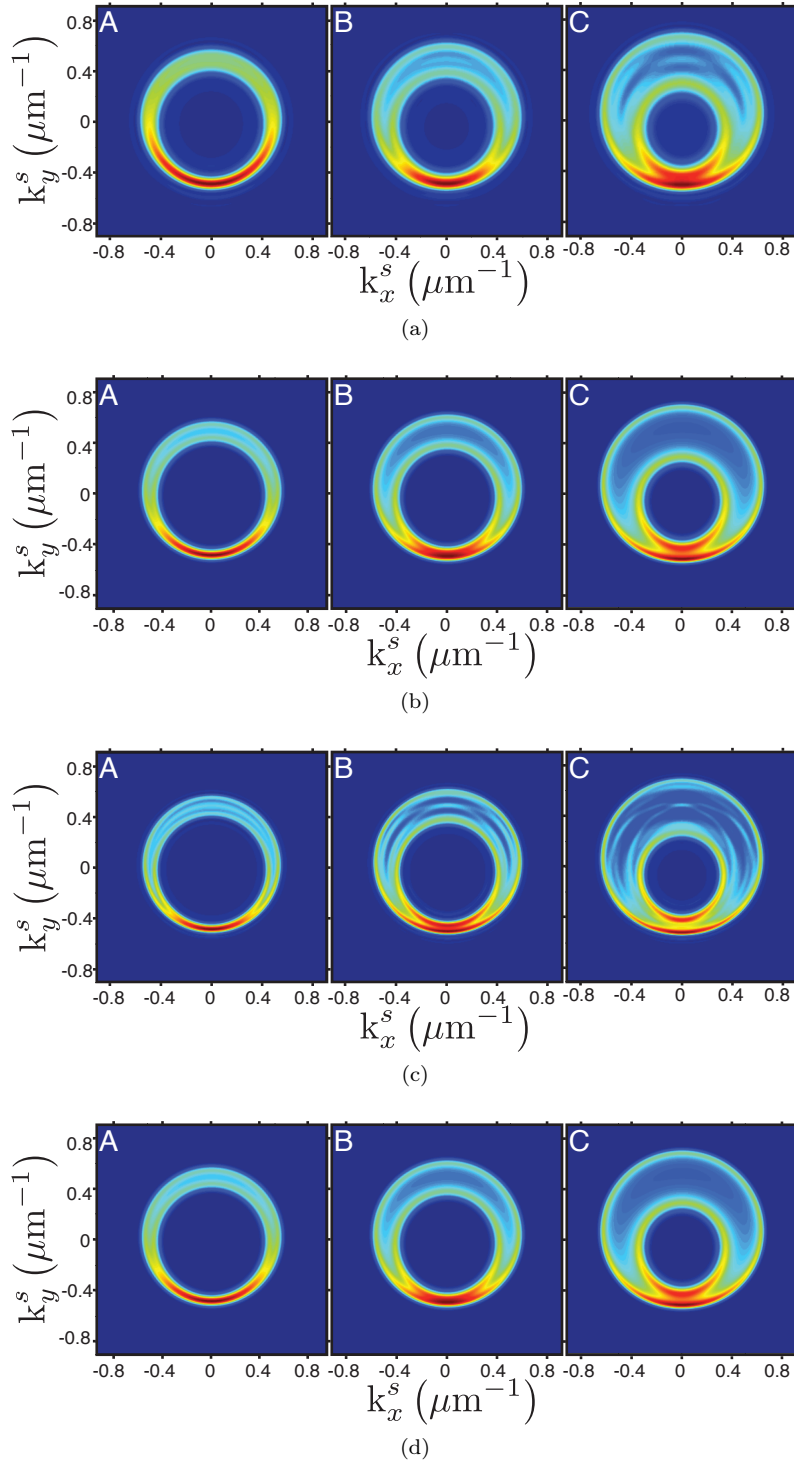


Figure 1: Angular spectrum (AS) for a pump beam with a waist $W = 0.0007\mu\text{m}^{-1}$ and different values of transverse wave number: (A) $\kappa_{\perp}^p = 0.05\mu\text{m}^{-1}$; (B) $\kappa_{\perp}^p = 0.09\mu\text{m}^{-1}$; (C) $\kappa_{\perp}^p = 0.15\mu\text{m}^{-1}$. Figures (a) and (b) consider a 1 mm long BBO crystal while in (c) and (d) the crystal length is increased to 2mm. In figures (a) and (c), the AS is calculated numerically through Eq.(9), while in figures (b) and (d) the AS is calculated from the analytic expression Eq.(23). The optical axis of the crystal is located in the Y-Z plane $\mathbf{a} \sim (0, 0.49, 0.87)$. For normal incidence the resulting walk-off angle is $\rho_{wo} \sim -\beta a_y \sim 0.068\text{rad}$ while the emission cones have a aperture angles around $\theta_A \sim r_{AS}/k_z^s \sim 0.034\text{rad}$, $r_{AS} \sim 0.49\mu\text{m}^{-1}$. The estimated transverse radii of the major emission cones are $R_+^A \sim 0.051\mu\text{m}^{-1}$, $R_+^B \sim 0.053\mu\text{m}^{-1}$ and $R_+^C \sim 0.056\mu\text{m}^{-1}$, while for the minor emission cones are $R_-^A \sim 0.042\mu\text{m}^{-1}$, $R_-^B \sim 0.036\mu\text{m}^{-1}$ and $R_-^C \sim 0.027\mu\text{m}^{-1}$; their centers are located at $A_{\pm}^A \sim \pm 0.02\mu\text{m}^{-1}$, $A_{\pm}^B \sim \pm 0.04\mu\text{m}^{-1}$ and $A_{\pm}^C \sim \pm 0.07\mu\text{m}^{-1}$.

related to the differences between the extraordinary and ordinary refractive indices and the other includes effects of the orientation of the birefringent axis \mathbf{a} . The latter is highly anisotropic and is directly related to the spatial walk-off. Both effects make evident that the idler photon characteristics can induce observable differences between the general characteristics of the signal photon with respect to the structured pump beam.

Since the condition of propagation invariance of a mode corresponds to restrict its wave vectors into a non necessarily homogenous cone, we observe that, whenever $\mathcal{R}_k^2 > 0$, the structure of Eq. (29) is that of an approximate propagation invariant signal photon, as reported in reference [14]. In the idealized limit of $W \rightarrow 0$,

$$R_c(\mathbf{k}_\perp^s, \omega^s; \mathbf{k}_\perp^i, \omega^i) \rightarrow \frac{|g\alpha(\omega_p)|^2}{k_\perp^0} \delta(|\mathbf{k}_\perp^s + \mathbf{k}_\perp^i| - \kappa_\perp^p) \times \text{Exp} \left[-\gamma^2 L^2 \left(2(\mathbf{k}_\perp^i + \mathbf{k}_\perp^s) \cdot \left(\frac{2c}{n_o \omega} \mathbf{k}_\perp^i - \beta \mathbf{a} \right) \left(\frac{\omega}{c} (n_{eff} - n_o) - \beta \mathbf{a} \cdot \mathbf{k}_\perp^i \right) + \frac{\omega}{c} (n_{eff} - n_o) - \beta \mathbf{a} \cdot \mathbf{k}_\perp^i \right)^2 \right]. \quad (31)$$

In this limit, the condition of propagation invariance for a beam with main propagation axis along $(2c/\omega n_o)(-\mathbf{k}_\perp^i, k_z^i)$ can be written as

$$\left[\frac{k_z^i}{k_\perp^i k_0^i} (\mathbf{k}_\perp^i \cdot \mathbf{k}_\perp^s) + \frac{k_\perp^i k_z^s}{k_0^i} \right]^2 + \left[\frac{\mathbf{k}_\perp^i \times \mathbf{k}_\perp^s}{k_\perp^i} \right]^2 = (\kappa_\perp^p)^2, \quad k_0^i = n_o \omega^i / c = |\mathbf{k}^i|; \quad (32)$$

expression that can also be written in the form

$$|\mathbf{k}_\perp^s + \mathbf{k}_\perp^i|^2 \left(\frac{\omega^i}{\omega^s} \right)^2 + (k_\perp^s)^2 \left[1 - \left(\frac{\omega^i}{\omega^s} \right)^2 \right] - \frac{(k_\perp^s)^2}{(k_0^i)^2} \left[(\mathbf{k}_\perp^i \cdot \hat{\mathbf{k}}_\perp^s)^2 + (k_\perp^i)^2 + \mathbf{k}_\perp^i \cdot \mathbf{k}_\perp^s \right] = \kappa_\perp^2. \quad (33)$$

As a consequence, the degenerate SPDC leads to approximate propagation invariant photons whenever $k_\perp^s \ll |\mathbf{k}^s|$. Under the experimental conditions reported in Ref. [14] $k_\perp^s / |\mathbf{k}^s| \sim 0.1$.

As we have shown, for paraxial pump beams, the mean radii of the AS cone is determined by the difference between refractive indices, while the radius κ_\perp of the modes that describe the emitted photons coincide with that of the pump Bessel beam.

In Fig. (2), the CAS function is illustrated using the same general parameters as in Fig. (1). We take the transversal wave vector of the idler photon $\mathbf{k}_\perp^{i,max}$ that maximizes the counts in the AS, and name it "maximal CAS". The results found for the AS let us expect that the maximum probability of emission of an idler photon would be obtained for $\mathbf{k}_{\perp,0}^{i,max} \sim (0, -r_{AS})$ where the two AS cones almost touch each other. In the case reported in Fig. (1a)A, the maximum AS corresponds to $\mathbf{k}_\perp^{i,max} = (0.027, -0.485) \mu\text{m}^{-1}$ and Fig. (2a) shows the corresponding maximal CAS. The transverse phase matching condition guarantees that the maximum probability signal photon wave vector will be located nearby the wave vector $-\mathbf{k}_{\perp,0}^{i,max}$ within a radius $\sim \kappa_\perp$. This region of the AS is where the two cones have the greatest separation. The propagation invariance structure of the pump beam makes that the CAS will also have an annular shape for $\mathbf{k}_\perp^{s,max}$ with a radius $\sim \kappa_\perp$. Since the AS nearby $-\mathbf{k}_{\perp,0}^{i,max}$ is quite asymmetric, the maximal CAS is also expected to be an asymmetric ring. In fact as κ_\perp increases, it may happen that the width and separation of the AS cones nearby the signal photon location are smaller than κ_\perp . Then the signal photon ring will not even close. The width of the ring is approximately equal to the width in wave vector space of the incident beam with a slight dependence on the crystal length, see Fig. (2b). Fig. (2c) illustrates the maximal CAS for an incident pump beam with a waist $W = 0.007 \mu\text{m}^{-1}$; it shows in greater detail its anisotropic transversal structure as a function of κ_\perp^p . The similarity with the experimental results reported in Ref.[14] is also evident.

Summarizing, the intensity structure of the maximal conditional spectrum is concentrated in a cone with an anisotropy that increases as κ_\perp^p increases. As a result, most conditionally emitted signal photons will be approximately propagation invariant but they will not correspond, in general, to Bessel-Gauss photons with a well defined ℓ value. Signal photons might be better approximated by Bessel-Gauss photons when paraxial pump beams are used.

B. Post selected photons with well defined angular momentum along different propagation axes.

Taking into account the results obtained in last section, it is relevant to study the angular momentum correlations of signal and idler photons. Thus, in this subsection, we consider the same general set up described in the previous subsection, and now evaluate the emission probability of photon pairs each of which has a Bessel-Gauss structure.

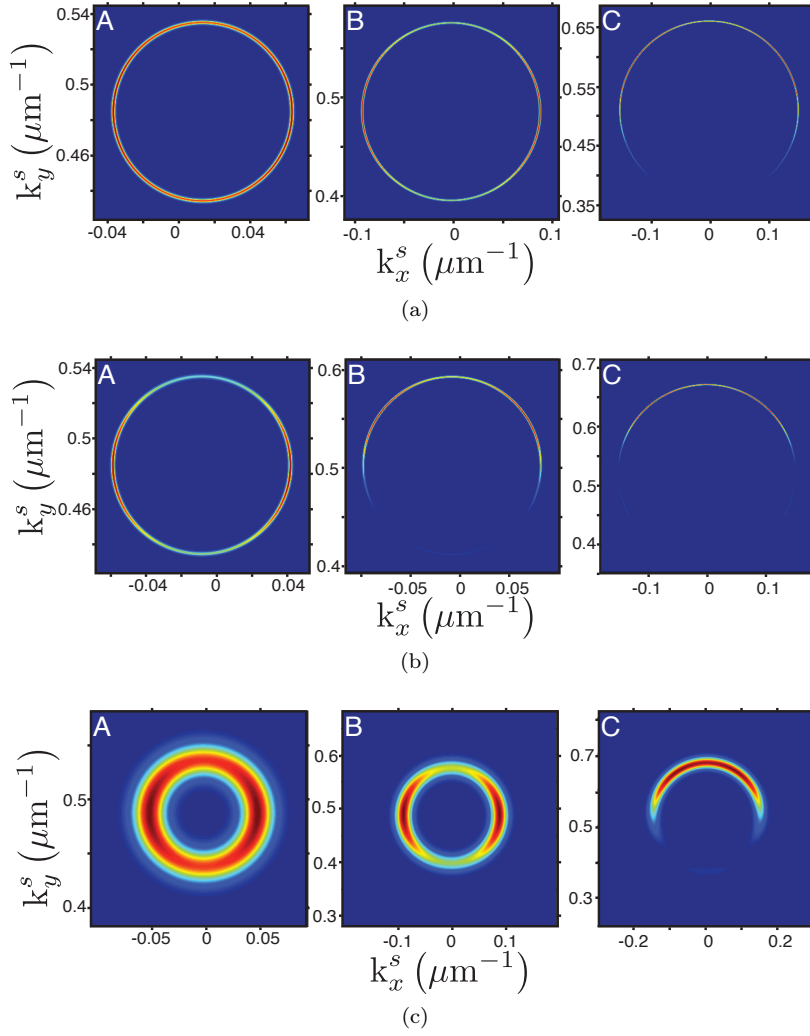


Figure 2: Maximal conditional angular spectrum for a pump Bessel Gauss beam with waist $W = 0.0007\mu\text{m}^{-1}$ in Figs. (a) and (b) and $W = 0.007\mu\text{m}^{-1}$ in Fig. (c). The transverse wave numbers are: (A) $\kappa_{\perp}^p = 0.05\mu\text{m}^{-1}$, (B) $\kappa_{\perp}^p = 0.09\mu\text{m}^{-1}$, and (C) $\kappa_{\perp}^p = 0.15\mu\text{m}^{-1}$. The crystal length is 1 mm in Figs. (a) and (c) and 2 mm in Fig. (b). The optical axis of the crystal is located in the Y - Z plane $\mathbf{a} \sim (0, 0.49, 0.87)$.

The calculation is made by a direct integration of Eq. (7) with the structured pump beam described by Eq. (5), and the idler and signal photons with the proper structure factor

$$\mathfrak{E}_{\mathbf{O},\kappa}(\mathbf{k}_x, \mathbf{k}_y; \omega) = \mathbf{a} \times \mathbf{k}^{\mathbf{O}} \tilde{\psi}_{\kappa}(\mathbf{k}_x, \mathbf{k}_y). \quad (34)$$

According to the results of last section, the main propagation axis of the post selected signal and idler Bessel photons is expected to differ from the pump beam axis. For a pump field close to satisfy the paraxial approximation, $\kappa_{\perp}^p \ll k_z^p$, this joint probability is expected to be maximal for photons with their main propagation axis nearby the cone with squared radius $r_{\text{AS}}^2 = (n_o\omega/c)^2 (1 - n_{\text{eff}}/n_o)/2$ in wave vector space. In Fig. (3), a schematic picture of the SPDC process under study in this section is shown.

Given a scalar Bessel beam with main propagation axis

$$\hat{p}_3 = (\sin \tilde{\theta} \cos \tilde{\varphi}, \sin \tilde{\theta} \sin \tilde{\varphi}, \cos \tilde{\theta}), \quad (35)$$

the vectors

$$\hat{p}_1 = (\cos \tilde{\theta} \cos \tilde{\varphi}, \cos \tilde{\theta} \sin \tilde{\varphi}, -\sin \tilde{\theta}), \quad (36)$$

$$\hat{p}_2 = (-\sin \tilde{\varphi}, \cos \tilde{\varphi}, 0), \quad (37)$$

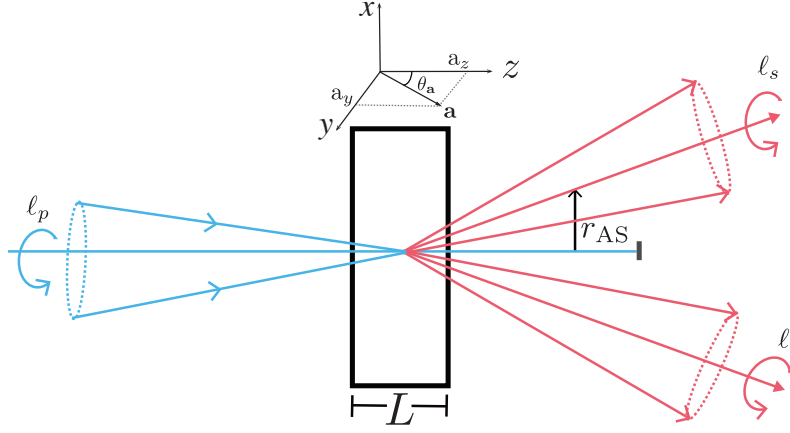


Figure 3: Schematic picture of the SPDC process involving propagation invariant pump, signal and idler photons with orbital angular momentum. The emission cone is expected to have a radii given by $r_{AS} = (n_o \omega / c)^2 (1 - n_{eff} / n_o) / 2$. The main propagation axis of the signal and idler photons will be approximately located on that cone.

together with (35) form an orthogonal basis on which any vector \mathbf{k} , with components (k_x, k_y, k_z) in the frame where the normal of the surface of the crystal coincides with the z -axis, has components

$$\begin{aligned}\tilde{k}_x &= k_x \cos \tilde{\theta} \cos \tilde{\varphi} + k_y \cos \tilde{\theta} \sin \tilde{\varphi} - k_z \sin \tilde{\theta} \\ \tilde{k}_y &= -k_x \sin \tilde{\varphi} + k_y \cos \tilde{\varphi} \\ \tilde{k}_z &= k_x \sin \tilde{\theta} \cos \tilde{\varphi} + k_y \sin \tilde{\theta} \sin \tilde{\varphi} + k_z \cos \tilde{\theta}.\end{aligned}\tag{38}$$

$$\tag{39}$$

In the basis $\{\hat{p}_1, \hat{p}_2, \hat{p}_3\}$ the scalar factor of the Bessel mode is

$$\psi_{\hat{p}_3; \kappa_\perp, \ell}(\tilde{\mathbf{r}}) = \int d^3 \tilde{\mathbf{k}} e^{i \tilde{\mathbf{k}} \cdot \tilde{\mathbf{r}}} \delta(\tilde{k}_z - \tilde{K}_z(\omega, \tilde{k}_\perp)) \frac{\delta(\tilde{k}_\perp - \kappa_\perp)}{\kappa_\perp} i^\ell e^{i \ell \tilde{\varphi}} \tag{40}$$

with \tilde{K}_z given by the adequate dispersion relation, Eqs. (18- 19). Writing the vector $\tilde{\mathbf{k}}$ in terms of (k_x, k_y, k_z) , and using that $\tilde{\mathbf{k}} \cdot \tilde{\mathbf{r}} = \mathbf{k} \cdot \mathbf{r}$, we can get an expression for $\tilde{\psi}_{\hat{p}_3; \kappa_\perp, \ell}(k_x, k_y)$. For an ordinary Bessel mode it results

$$\begin{aligned}\tilde{\psi}_{\hat{p}_3; \kappa_\perp, \ell}^{(O)}(\mathbf{k}) &= \pm \frac{k_\perp^{|\ell|}}{\kappa_\perp^{|\ell|}} \frac{\delta(k_z - K_z^{(O)}(\omega_B, \kappa_\perp, \tilde{\theta}; \varphi))}{\kappa_\perp} \frac{\delta(k_\perp - K_\perp^{(O)}(\kappa_\perp, \omega_B, \tilde{\theta}; \varphi))}{\text{Jac}^{(O)}(\kappa_\perp, \omega_B, \tilde{\theta}; \varphi)} \\ &\times \sum_{m=0}^{|\ell|} \binom{|\ell|}{m} \left(\cos \tilde{\theta} \cos(\varphi - \tilde{\varphi}) + i \frac{\ell}{|\ell|} \sin(\varphi - \tilde{\varphi}) \right)^m \left(-\frac{k_z}{k_\perp} \sin \tilde{\theta} \right)^{|\ell|-m}.\end{aligned}\tag{41}$$

$$K_z^{(O)}(\kappa_\perp, \omega_B; \varphi; \tilde{\theta}; \tilde{\varphi}) = \left[\frac{\sqrt{\epsilon_\perp \omega_B^2 / c^2 - \kappa_\perp^2}}{\cos \tilde{\theta}} \right]$$

$$\pm |\tan \tilde{\theta} \cos(\tilde{\varphi} - \varphi)| \sqrt{\kappa_\perp^2 / \cos^2 \tilde{\theta} - (\epsilon_\perp \omega_B^2 / c^2) \tan^2 \tilde{\theta} \sin^2(\tilde{\varphi} - \varphi)} / (1 + \tan^2 \tilde{\theta} \cos^2(\tilde{\varphi} - \varphi)), \tag{42}$$

$$K_\perp^{(O)}(\kappa_\perp, \omega_B; \varphi; \tilde{\theta}; \tilde{\varphi}) = \sqrt{\epsilon_\perp \omega_B^2 / c^2 - K_z^{(O)2}}, \tag{43}$$

and the Jacobian term is

$$\text{Jac}^{(O)}(\omega_B; \kappa_\perp; \varphi; \tilde{\theta}, \tilde{\varphi}) = \frac{|\kappa_\perp - k_z \cos(\tilde{\varphi} - \varphi) \sin \tilde{\theta}|}{\kappa_\perp}. \tag{44}$$

The dependence of the relevant values of k_z and k_\perp , $K_z^{(O)}$ and $K_\perp^{(O)}$, on the angle φ reflects the elliptic shape of the beam in the wave vector plane defined by a constant value of k_z . The ordinary dispersion relation term $\sqrt{\epsilon_\perp \omega_B^2/c^2 - \kappa_\perp^2}$ is a direct measure of the electromagnetic momentum of the Bessel beam along the \hat{p}_3 axis. $K_z^{(O)}$ is proportional to the momenta along the z -axis; κ_\perp determines directly the radial momenta of ordinary photons perpendicular to the \hat{p}_3 axis; the Jacobian terms Eq. (44) are a consequence of the conceptual difference between k_\perp and κ_\perp . Note that the effective dispersion relation for the Bessel mode, Eq. (42) gives real values just for values of the angular variable φ satisfying $|\kappa_\perp| \geq |(n_o \omega_B/c) \sin \tilde{\theta}|$. The summation terms in Eq. (41) substitute the $e^{i\ell\varphi}$ term that would arise for a Bessel beam propagating along the \hat{e}_3 -axis. Notice that similar terms arise in the description of SPDC for other beams exhibiting orbital angular momentum as, for instance, Laguerre Gaussian beams [10].

The transition amplitude of the generation of a signal Bessel photon with angular momenta ℓ^s and transverse wave number κ_\perp^s along with an idler Bessel photon with angular momenta ℓ^i and transverse wave number κ_\perp^i is proportional to

$$F(\ell^p, \kappa_\perp^p, \omega^p; \ell^s, \kappa_\perp^s, \omega^s; \ell^i, \kappa_\perp^i, \omega^i) = \int d^3\mathbf{k}^s \int d^3\mathbf{k}^i \tilde{\psi}_{\hat{e}_3; \kappa_\perp^p, \ell^p}^{(E)}(\mathbf{k}_\perp^i + \mathbf{k}_\perp^s; \ell^p) \tilde{\psi}_{\hat{p}^s; \kappa_\perp^s, \ell^s}^{(O)}(\mathbf{k}_\perp^s) \tilde{\psi}_{\hat{p}^i; \kappa_\perp^i, \ell^i}^{(O)}(\mathbf{k}_\perp^i) \text{sinc}(L\Delta k_z/2); \quad (45)$$

the proportionality factor $g = |\alpha| \mathcal{N}_p \mathcal{N}_s \mathcal{N}_i \mathcal{X}_{eff}$ involves the pump coherent amplitude α , the normalization factors of the pump, idler and signal photons as well as the adequate effective nonlinear susceptibility.

According to the results of last section, the transition amplitude will become maximal if the signal photon has an orientation axis $\hat{p}_3^{(s)}$ determined by the maxima in the AS function, while the orientation of the idler photon corresponds to $\tilde{\theta}_i = \tilde{\theta}_s$ and $\tilde{\varphi}_i = \tilde{\varphi}_s + \pi$ provided that $\kappa_\perp^s < \kappa_\perp^i$. The anisotropy of the AS has as a consequence that the general features of the photon pairs depend also on their emission orientation. Notice also that in this scheme the idler and signal photons could be distinguished by their perpendicular wave vector.

In Figs. (4) and (5) we illustrate the behavior of the conditional amplitudes as a function of the angular momentum of the pump photon as well as a function of its transverse wave vector. In those figures we also illustrate the dependence on the orientation of the resulting idler and signal photons. To make the results closer to expected experimental realizations, the calculations were performed with Bessel-Gauss modes with a small waist $W = 0.0005 \mu\text{m}^{-1}$. The crystal properties are the same as in the illustrative examples of the CAS and AS distributions in last section.

As could be inferred from the results obtained for the CAS, smaller values of the pump transverse vector κ_\perp^p yield a more localized distribution of the OAM of the photon pair. That is, pump beams that can be closely described by the paraxial approximation can be used to generate photon pairs with few relevant values of ℓ^i and ℓ^s . In particular, a paraxial pump beam with $\ell^p = 0$ will yield mainly photon pairs without OAM along their propagation axis.

For pump beams with bigger κ_\perp^p it is predicted a high correlation between the angular momentum of the idler and signal photons involving a broad but well defined values ℓ^i and ℓ^s along a straight line. This property is preserved whether the structured photon pairs are detected in the direction of maximal CAS (first row in Figs. (4) and (5)) or in any other orientation as illustrated in the second row in Figs. (4) and (5). For paraxial beams, the maximum transition rates for an orientation perpendicular to that of maximal CAS is approximately half of the maximum values found along the maximal CAS.

Notice that as the orbital angular momentum is evaluated along different axes for the idler, signal and pump photons, it does not make strict sense to talk about conservation of OAM by comparing $\ell^i + \ell^s$ with ℓ^p . Nevertheless we can observe that the greatest transition rates in the non paraxial regime, Fig. (5), are along straight lines that go through the origin for $\ell^p = 0$, pass through $|\ell^i| = 1$ and $\ell^s = 0$ for $\ell^p = 1$, and pass through $|\ell^i| = 2$ and $\ell^s = 0$ for $\ell^p = 2$. For photon pairs emitted in an orientation perpendicular to that of maximal CAS this property is more evident. This could be a consequence of the fact that in this orientation the AS is more symmetric under the change $\tilde{\varphi}' = \tilde{\varphi} + \pi$, as illustrated in Fig. 1.

Finally, in Fig. (6), the marginal distributions of the idler and signal orbital angular momentum are illustrated. They were evaluated for a paraxial pump beam with the same set up as in Fig. (4). For the photon in the pair with the same value of κ_\perp than the pump beam, i. e., for idler photon, the OAM marginal distribution has clearly an oscillatory behavior dependent on the parity of the ℓ^i for $-15 \leq \ell^i \leq 15$. Meanwhile, for the photon with lower value of κ_\perp this behavior is observed for a much smaller ℓ^s interval.

IV. CONCLUSIONS

In this paper, it has been shown that SPDC can be used to generate structured photons with several predetermined properties inherited from the pump beam. We have found that the use of scalar pump fields that are approximately

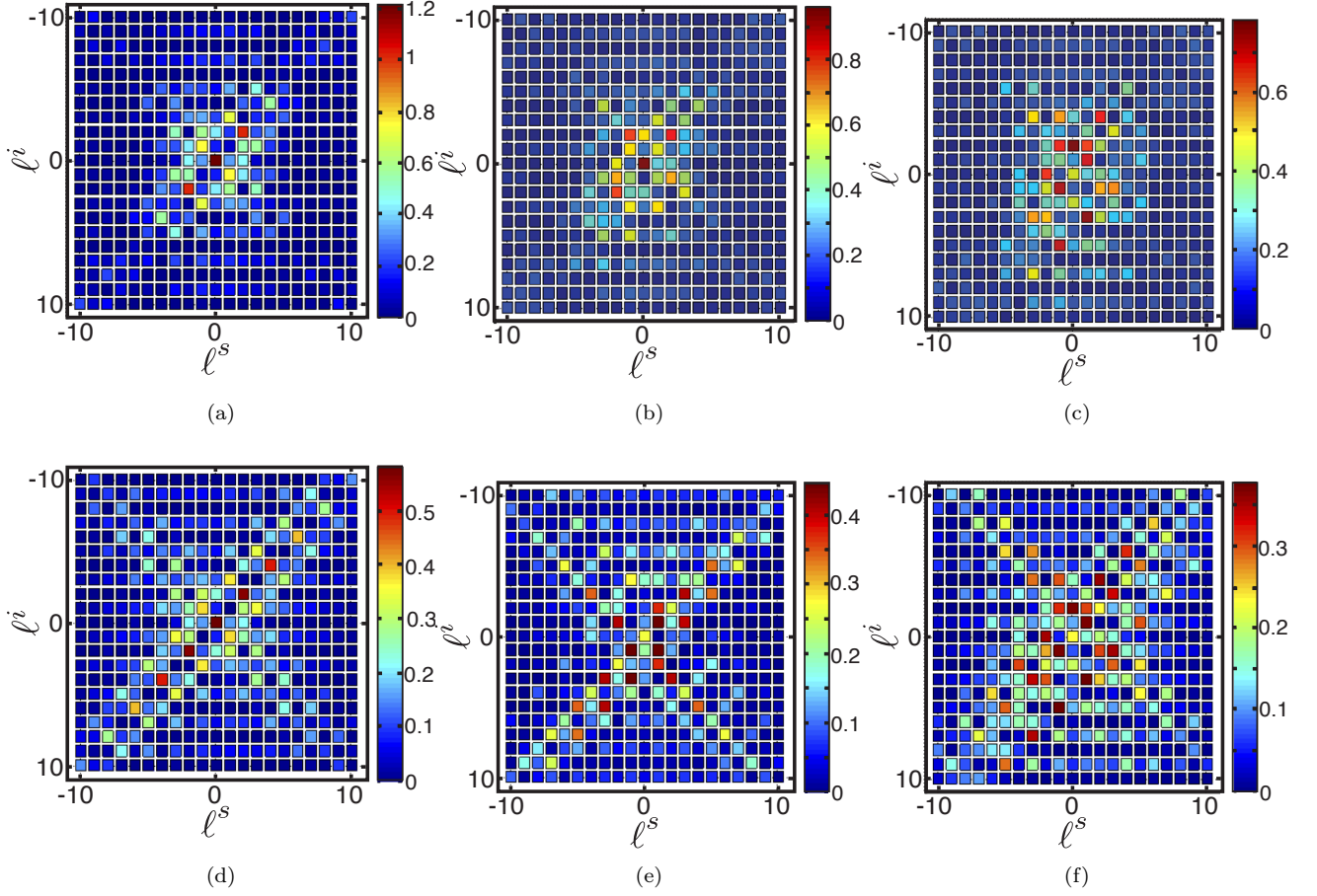


Figure 4: Modulus of the transition element F , Eq. (45), as a function of the orbital angular momentum of the signal ℓ^s and idler ℓ^i photon. They involve a pump Bessel Gauss photon with transverse wave number $\kappa_{\perp}^p = 0.01\mu\text{m}^{-1}$, a signal Bessel photon with $\kappa_{\perp}^s = 0.0001\mu\text{m}^{-1}$ and an idler photon with $\kappa_{\perp}^i = 0.01\mu\text{m}^{-1}$. The idler and signal photons are emitted with their main propagation axis with orientation angles $\tilde{\theta} = \theta_{ec}$ and $\tilde{\varphi}_s = -\pi/2$ and $\tilde{\varphi}_i = \pi/2$ for the first row, while $\tilde{\varphi}_s = 0$ and $\tilde{\varphi}_i = \pi$ in the second row. The pump angular quantum number is $\ell^p = 0$ in figures (a) and (d), $\ell^p = 1$ in figures (b) and (e), and $\ell^p = 2$ in figures (c) and (f). The BBO crystal length is 1mm, its optical axis is located in the Y - Z plane, and the width of the transversal wave number for the Bessel-Gauss photons is $W = 0.0005\mu\text{m}^{-1}$. The optical axis of the crystal is located in the Y - Z plane $\mathbf{a} \sim (0, 0.49, 0.87)$.

propagation invariant can be used to generate heralded single photons with the same property. A detailed study of type I spontaneous down conversion (SPDC) of Bessel-Gauss photons was performed as an interesting example for the study of generation of structured photons from beams that are propagation invariant and also have OAM. Explicit analytical and numerical results were given for the angular and conditional spectrum using a birefringent crystal cut with the optical axis optimized for SPDC with standard Gaussian pump beams. Since the AS and the CAS do not depend on the detailed phase structure of the pump beam in the wave vector domain, the results obtained in this work are expected to be valid for other structured pump beams such as Mathieu and Weber beams.

It was also shown that, as the magnitude of the transverse wave vector of a pump Bessel-Gauss beam increases, the emission cone is deformed into two non coaxial cones which touch each other along a line determined by the orientation of the optical axis of the nonlinear crystal. At this location, the conditional spectrum becomes maximal for a pair of photons, one of which is best described in wave vector space by a Gaussian like photon, with a very small transverse wave vector, and the other by a Bessel-Gauss photon with the same mean and width distribution of transverse wave vectors as the incident pump photon. Both of them have their main propagation axis close to the cone expected for a Gaussian pump beam. The results were successfully compared with reported experiments.

The study on the OAM distribution for the photon pairs showed the existence of clear correlations in the OAM quantum number of the idler and signal photons. These correlations can be manipulated by varying the pump

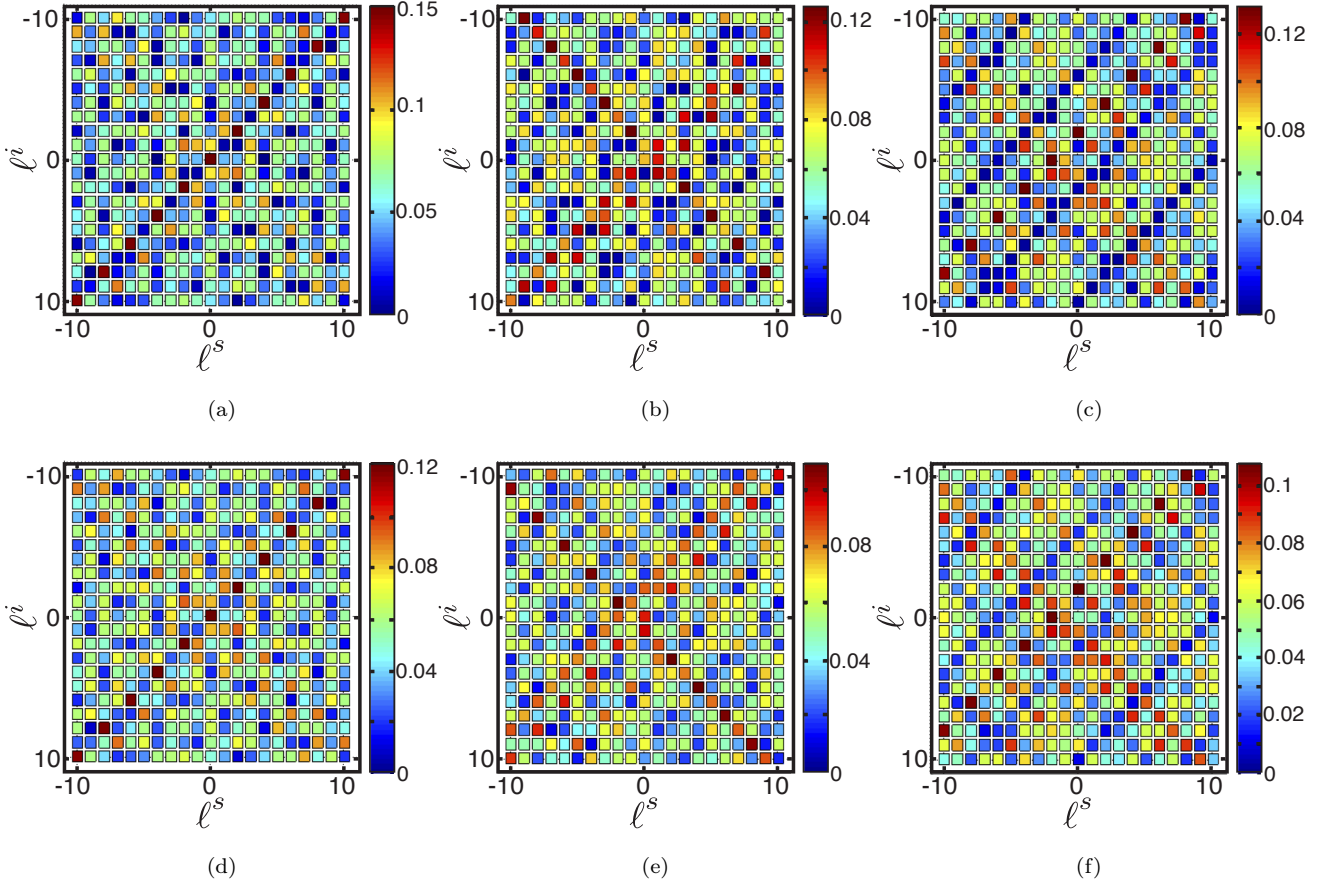


Figure 5: Modulus of the transition element F , Eq. (45), as a function of the orbital angular momentum ℓ^s of the signal and ℓ^i of the idler photon. They involve a pump Bessel Gauss photon with transverse wave number $\kappa_{\perp}^p = 0.05\mu\text{m}^{-1}$, a signal Bessel photon with $\kappa_{\perp}^i = 0.001\mu\text{m}^{-1}$ and an idler photon with $\kappa_{\perp}^i = 0.05\mu\text{m}^{-1}$. The idler and signal photons are emitted with their main propagation axis with orientation angles $\hat{\theta} = \theta_{ec}$ and $\hat{\varphi}_s = -\pi/2$ and $\hat{\varphi}_i = \pi/2$ in the first row, while $\hat{\varphi}_s = 0$ and $\hat{\varphi}_i = \pi$ in the second row. The pump angular quantum number is $\ell^p = 0$ in figures (a) and (d), $\ell^p = 1$ in figures (b) and (e) and $\ell^p = 2$ in figures (c) and (f). The BBO crystal length is 1mm, its optical axis is located in the Y - Z plane and the width of the transversal wave number for the Bessel-Gauss photons is $W = 0.0005\mu\text{m}^{-1}$. The optical axis of the crystal is located in the Y - Z plane $\mathbf{a} \sim (0, 0.49, 0.87)$.

parameters κ_{\perp}^p and ℓ^p . They also depend on the orientation of the photon pair main propagation axes. The OAM significant correlations involve a smaller number of ℓ^s and ℓ^i values for paraxial pump beams. This means that heralded values of ℓ^s , given a particular value of ℓ^i , could be easily obtained in that regime. However, even for relatively high values of κ_{\perp}^p , we observe some interesting OAM correlation features. In particular, there is a trend to preserve parity (the value of $\ell^s + \ell^i$ for the most probable photon pairs have the same parity that ℓ^p). This effect results evident from the analysis of the marginal correlations. There is also a trend to get the greatest transition rates along straight lines in the ℓ^s - ℓ^i space. These lines pass, in general, through the ℓ^p value. Finally, it has also been shown that the OAM correlations cannot be interpreted in terms of angular momentum conservation.

-
- [1] L. Allen, M. W. Beijersbergen, R. J. C. Spreeuw, and J. P. Woerdman, Phys. Rev. A **45**, 8185 (1992).
 - [2] K. Volke-Sepúlveda, V. Garcés-Chávez, S. Chávez-Cerda, J. Arlt and K. Dholakia, J. Opt. B: Quantum Semiclass. Opt. **S82**, 1464 (2002).
 - [3] C. López-Mariscal, M. A. Bandres, J. C. Gutiérrez-Vega, Opt. Eng. **45**, 068001 (2006).
 - [4] B. M. Rodríguez-Lara and R. Jáuregui, Phys. Rev A **79**, 055806 (2009); C. L. Hernández-Cedillo, S. Bernon, H. Hatter-

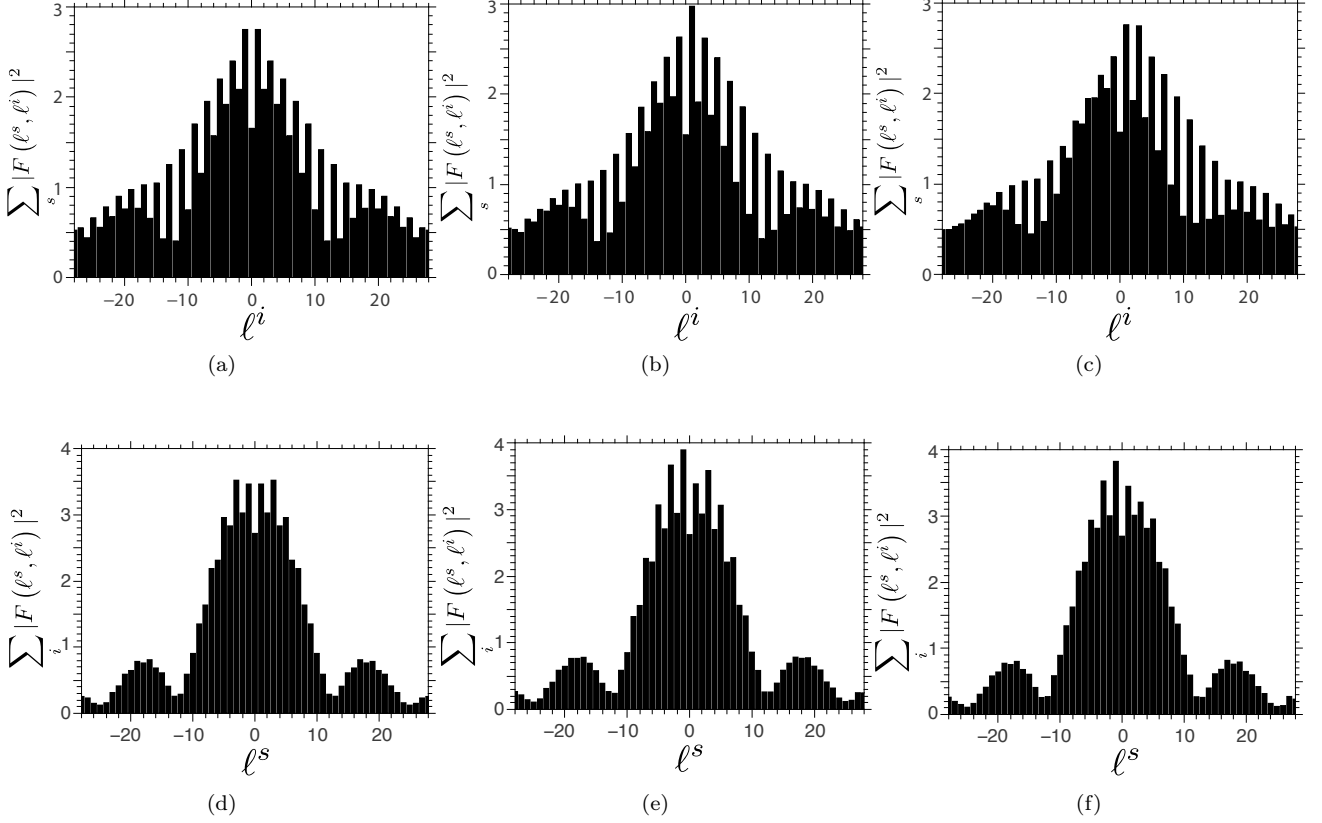


Figure 6: Marginal distribution of orbital angular momentum of the signal ℓ^s and idler ℓ^i photon. They involve a pump Bessel Gauss profile with transverse wave number $\kappa_{\perp}^p = 0.01\mu\text{m}^{-1}$, a signal Bessel photon with $\kappa_{\perp}^s = 0.0001\mu\text{m}^{-1}$ and an idler photon with $\kappa_{\perp}^i = 0.01\mu\text{m}^{-1}$. The idler and signal photons are emitted with their main propagation axis with orientation angles $\tilde{\theta} = \theta_{ec}$ and $\tilde{\varphi}_s = -\pi/2$ and $\tilde{\varphi}_i = \pi/2$. The pump angular quantum number is $\ell^p = 0$ in figures (a) and (d), $\ell^p = 1$ in figures (b) and (e), and $\ell^p = 2$ in figures (c) and (f). The BBO crystal length is 1 mm, its optical axis is located in the Y - Z plane and the width of the transversal wave number for the Bessel-Gauss photons is $W = 0.0005\mu\text{m}^{-1}$. The optical axis of the crystal is located in the Y - Z plane $\mathbf{a} \sim (0, 0.49, 0.87)$.

- mann, J. Fortágh, R. Jáuregui, Phys. Rev. A **87**, 023404 (2013).
- [5] G. A. Siviloglou, J. Broky, A. Dogariu, and D. N. Christodoulides, Phys. Rev. Lett. **99**, 213901 (2007).
- [6] P. G. Kwiat, K. Mattle, H. Weinfurter, A. Zeilinger, A. V. Sergienko, and Y. Shih, Phys. Rev. Lett. **75**, 4337 (1995).
- [7] H. Bechmann-Pasquinucci and W. Tittel, Phys. Rev. A **61**, 062308 (2000).
- [8] Al. Mair, A. Vaziri, G. Weihs, and A. Zeilinger, Nature **412**, 313 (2001).
- [9] S. Hacyan and R. Jáuregui, Journal of Optics A: Pure and Applied Optics **11**, 085204 (2009).
- [10] C. I. Osorio, G. Molina-Terriza, and J. P. Torres, Phys. Rev. A **77**, 015810 (2008).
- [11] S. P. Walborn, C. H. Monken, S. Pádua and P. H. Souto Ribeiro, Physics Reports **495**, 87 (2010).
- [12] M. V. Fedorov, M. A. Efremov, P. A. Volkov, E. V. Moreva, S. S. Straupe, and S. P. Kulik, Phys. Rev. A **77** 032336 (2008).
- [13] A. V. Burlakov, M. V. Chekhova, D. N. Klyshko, S. P. Kulik, A. N. Penin, Y. H. Shih, and D. V. Strekalov, Phys. Rev. A **56**, 3214 (1997); C. H. Monken, P. H. Souto Ribeiro, and S. Pádua, Phys. Rev. A **57**, 3123 (1998).
- [14] H. Cruz-Ramírez, R. Ramírez-Alarcón, F. J. Morelos, P. A. Quinto-Su, J. C. Gutiérrez-Vega, and A. B. U'Ren, Opt. Express **20**, 29761 (2012).
- [15] F. A. Bovino, P. Varisco, A. M. Colla, G. Castagnoli, G. di Guiseppe, and A. V. Sergeinko, Opt. Commun. **227**, 343 (2003).
- [16] Z. Bouchal, J. Wagner and M. Chlup, Opt. Commun. **151**, 207 (1998).
- [17] C. K. Hong and L. Mandel, Phys. Rev. A **31**, 2409 (1985).
- [18] The description of structured light in terms of scalar modes is necessarily approximate. Linear polarized Bessel modes have necessarily a component of the electric field along the main direction of propagation that can be neglected in the paraxial

- approximation. See, e. g. R. Jáuregui and S. Hacyan, Phys. Rev. A **71**, 033411 (2005).
- [19] V. G. Dmitriev, G. G. Gurzadyan, D. N. Nikogosyan, *Handbook of Nonlinear Optical Crystals*, Third Edition, Springer-Verlag, Berlin (1999).
 - [20] That is not the case for Laguerre-Gaussian beams taken as pump beams in SPDC. They are paraxial beams that also carry orbital angular momentum; their angular spectra contains a factor k_{\perp}^{n+2m} that yields a dependence on m of the corresponding joint amplitude
 - [21] S. P. Walborn, A. N. de Oliveira, R. S. Thebaldi, and C. H. Monken, Phys. Rev. A **69**, 023811 (2004).
 - [22] J. P. Torres, G. Molina-Terriza, and L. Torner, J. Opt. B **7**, 235 (2005).
 - [23] A. G. da Costa Moura, W. A. T. Nogueira, S. P. Walborn and C. H. Monken, arXiv:0806.4624v1 (2008).
 - [24] L. E. Vicent, A. B. U'Ren, R. Rangarajan, C. I. Osorio, J. P. Torres, L. Zhang and I. A. Walmsley, New J. Phys. **12**, 093027 (2010).
 - [25] Y. Jerónimo-Moreno and R. Jáuregui, J. Opt. **16**, 065201 (2014).